Materials Today Physics 20 (2021) 100452

Contents lists available at ScienceDirect

Materials Today Physics

journal homepage: https://www.journals.elsevier.com/materials-today-physics

Realizing high doping efficiency and thermoelectric performance in *n*-type SnSe polycrystals *via* bandgap engineering and vacancy compensation

Lizhong Su [a], Tao Hong [a], Dongyang Wang [a], Sining Wang [a], Bingchao Qin [a], Mengmeng Zhang [a], Xiang Gao [b], Cheng Chang [c,*], Li-Dong Zhao [a,**]

[a] School of Material Science and Engineering, Beihang University, Beijing, 100191, China
[b] Center for High Pressure Science and Technology Advanced Research (HPSTAR), Beijing, 100094, China
[c] Institute of Science and Technology Austria, Am Campus 1, 3400, Klosterneuburg, Austria

ARTICLE INFO

Article history:
Received 22 May 2021
Received in revised form
27 May 2021
Accepted 27 May 2021
Available online 3 June 2021

Keywords:
Thermoelectric
SnSe
Bandgap
Formation energy
Transition energy

ABSTRACT

SnSe, a wide-bandgap semiconductor, has attracted significant attention from the thermoelectric (TE) community due to its outstanding TE performance deriving from the ultralow thermal conductivity and advantageous electronic structures. Here, we promoted the TE performance of *n*-type SnSe polycrystals through bandgap engineering and vacancy compensation. We found that PbTe can significantly reduce the wide bandgap of SnSe to reduce the impurity transition energy, largely enhancing the carrier concentration. Also, PbTe-induced crystal symmetry promotion increases the carrier mobility, preserving large Seebeck coefficient. Consequently, a maximum *ZT* of ~1.4 at 793 K is obtained in Br doped SnSe−13% PbTe. Furthermore, we found that extra Sn in *n*-type SnSe can compensate for the intrinsic Sn vacancies and form electron donor-like metallic Sn nanophases. The Sn nanophases near the grain boundary could also reduce the intergrain energy barrier which largely enhances the carrier mobility. As a result, a maximum *ZT* value of ~1.7 at 793 K and an average *ZT* (ZT_{ave}) of ~0.58 in 300−793 K are achieved in Br doped $Sn_{1.08}Se$−13%PbTe. Our findings provide a novel strategy to promote the TE performance in wide-bandgap semiconductors.

1. Introduction

Thermoelectric (TE) technology, which achieves direct conversion between thermal energy and electric energy, is a potential environmentally friendly technology of power generation and refrigeration [1,2]. The property of TE material is determined by the dimensionless figure of merit $ZT = S^2\sigma T/(\kappa_{lat} + \kappa_{ele})$, where S is the Seebeck coefficient, σ is the electrical conductivity, T is the temperature in Kelvin, κ_{lat} is the lattice thermal conductivity and κ_{ele} is the electron thermal conductivity, respectively [3,4]. Understandably, researchers pursue higher power factor ($PF = S^2\sigma$) and lower total thermal conductivity ($\kappa_{tot} = \kappa_{lat} + \kappa_{ele}$) to optimize the TE performance. However, it is challenging to simultaneously improve the electrical performance and decrease thermal conductivity due to the intricate interrelationship between these TE parameters [5]. After decades of efforts, several effective strategies have emerged to enhance the TE performance, including band structure engineering [6–9], all-scale hierarchical architectures [10–13], and exploiting materials with intrinsically low thermal conductivity [14–20]. Notably, these strategies are developed on the basis of the optimized carrier concentration of 10^{19}-10^{20} cm^{-3}. In the past decades, PbQ (Q = Te, Se, S) and Bi_2Te_3, known as typical narrow-bandgap semiconductors, are extensively investigated and great progress has been made [21] because their carrier concentrations can be easily tuned to the desired range by applying several efficient donor- or accepter-like dopants. However, wide-bandgap semiconductors, which could be more promising than narrow-bandgap semiconductors as wide-temperature TE materials [22], have long been underestimated due to the unsatisfying dopants and carrier concentration. For example, the electron concentration of 0.18% Br doped PbSe polycrystal is ~3 × $10^{19}cm^{-3}$, while the electron concentration is only 1.3 × $10^{19}cm^{-3}$ in 12% Br doped SnSe [23,24].

* Corresponding author.
** Corresponding author.
E-mail addresses: cheng.chang@ist.ac.at (C. Chang), zhaolidong@buaa.edu.cn (L.-D. Zhao).

https://doi.org/10.1016/j.mtphys.2021.100452
2542-5293/

Here, we present effective strategies to increase the doping efficiency in *n*-type SnSe by bandgap engineering and intrinsic vacancy compensation.

SnSe is a wide-bandgap semiconductor with an intrinsically low thermal conductivity due to its strong anharmonic and anisotropic bonding [25,26]. The ultralow thermal conductivity and unique band structure enable excellent TE performance in both *p*-type and *n*-type SnSe crystals [27–30]. For *p*-type SnSe crystal, the carrier concentration of SnSe crystal increased from ~3 × 10^{17} cm^{-3} to ~4 × 10^{19} cm^{-3} by Na doping, successfully pushing the Fermi level downward the multiple valance bands and thus activating the multiple-bands transport. For *n*-type SnSe crystal, Br doping converts SnSe crystal to *n*-type with a high carrier concentration of 1.2 × 10^{19} cm^{-3}. The overlapping interlayer charge density facilitates electron transport through the interlayers and enables high out-of-plane charge transport. Although SnSe crystal reveals excellent TE performance, its poor mechanical properties limit large-scale commercial applications, which motivates us to optimize the TE performance of SnSe polycrystals. In recent years, several high-performance SnSe polycrystals have been reported [31–38]. Nonetheless, the electrical properties of *n*-type SnSe polycrystals are still unsatisfactory with low carrier concentration or low carrier mobility. A higher *ZT* could be expected if the carrier concentration and carrier mobility could be further increased.

The carrier concentration in doped semiconductors is mainly determined by the state of dopants, $n = g_q e^{-E_f/k_B T}$, where g_q is the degeneracy factor, E_f is the formation energy of dopants [39]. It is evident that low formation energy is critical for higher doping efficiency. Specifically, Na and Br are impurities with relatively low formation energy [39]. The other factor that influences the doping effect is the transition energy level which also determines the role of dopant as a donor or an acceptor. Transition energy presents the energy of transferring an electron between the impurity center and the valence or conduction band. Generally, the dopant transition energy level tends to donate electrons to conduction band minimum (CBM) rather than to accept electrons from valence band maximum (VBM) if it is close to the CBM, oppositely, it tends to accept electrons from VBM rather than donate electrons to CBM if it is close to VBM [40]. If the impurity state is deeply inside the bandgap, high energy is needed to activate the charge carriers to VBM or CBM, that is to say, impurities with high transition energy levels tend to form electron traps and inhibit the formation of free carriers. Therefore, the effective dopant should possess low formation energy and low transition energy level simultaneously. Na meets the requirements and presents high doping efficiency in *p*-type SnSe [41], however, Br has much higher transition energy according to our DFT calculations, partly contribute to the low doping efficiency in *n*-type SnSe.

In this work, we applied PbTe alloying to reduce the transition energy level of Br in SnSe (SnSe mentioned below refers to 3% Br-doped SnSe polycrystals). PbTe successfully reduced the wide bandgap of SnSe, which shallows the impurity level and thus results in enhanced carrier concentration. The bandgap is reduced from 0.84 eV in SnSe to 0.74 eV in $Sn_{0.85}Pb_{0.15}Se_{0.85}Te_{0.15}Br_{0.03}$ (labeled as SnSe+15%PbTe). As a result, the carrier concentration increased from 1.83 × $10^{18}$$cm^{-3}$ to 1.36 × 10^{19} cm^{-3}. Meanwhile, the carrier mobility and Seebeck coefficient obtain a moderate increase due to the modified crystal symmetry and valence bands energy offset. The synergistic effects lead to a maximum *ZT* of 1.4 at 793 K in SnSe−13%PbTe with 1.0 × 10^{19} cm^{-3}. Furthermore, we found extra Sn can also optimize the carrier concentration significantly. The intrinsic Sn vacancies in *n*-type SnSe act as electron traps reducing the free electron concentration. Extra Sn compensates the vacancies by increasing the Sn vacancy formation energy and also forms the metallic Sn nanophases which could donate electrons to SnSe matrix. Consequently, the highest carrier concentration at room temperature of 1.38 × 10^{19} cm^{-3} is obtained in $Sn_{1.08}$Se−13%PbTe. Furthermore, the Sn nanophases at the grain boundary could reduce the intergrain energy barrier, largely increasing the carrier mobility [42]. The room temperature carrier mobility increases from 0.6 $cm^2V^{-1}s^{-1}$ in SnSe to 4.2 $cm^2V^{-1}s^{-1}$ in $Sn_{1.08}$Se−13%PbTe. Combined with the low thermal conductivity, the maximum *ZT* (ZT_{max}) reaches ~1.7 at 793 K with an average *ZT* (ZT_{ave}) of ~0.58 in 300–793 K. These findings provide a novel strategy to promote the TE performance in wide-bandgap semiconductors.

2. Results and discussions

SnSe belongs to space group *Pnma* with a layered structure at room temperature. With the rising temperature, a continuous phase transition appears which results in the space group of SnSe transforming from *Pnma* to *Cmcm* [43,44]. The powder XRD patterns of SnSe-x%PbTe and Sn_{1+y}Se-13%PbTe samples are shown in Fig. 1. The ultrahigh peak intensity at 31° corresponds to the (400) plane, revealing the highly textured structure in all samples, which is proven by SEM in Figure S1. The XRD peaks shift to low angles with increasing PbTe amount, indicating that PbTe alloyed with SnSe. In contrast, the XRD peaks nearly unchanged with increasing extra Sn amount, indicating that extra Sn may form second phases. Fig. 1c–d shows the calculated lattice parameters of SnSe-x%PbTe and Sn_{1+y}Se-13%PbTe samples, which are in accordance with the XRD peak changes.

Fig. 2 shows the electrical transport properties of SnSe-x%PbTe and Sn_{1+y}Se-13%PbTe samples (unless otherwise noted, all the thermal and electrical properties are measured along with the direction parallel to the SPS pressing (*P*) direction in this work [28]. The TE performance along two directions can be found in SI, Figure S2). After two-step optimizations, the electrical conductivity of Br-doped SnSe polycrystals improved obviously in the whole temperature region of 300–793 K, as shown in Fig. 2a. A high electrical conductivity of ~52 S cm^{-1} is achieved at 793 K in SnSe−13%PbTe. The electrical conductivity further increases to ~60 S cm^{-1} at 793 K with 8% Sn.

The electrical conductivity enhancement results from the synergistic optimization of carrier mobility and carrier concentration, as shown in Fig. 2b. After PbTe alloying, the room-temperature carrier concentration increases from 1.83 × 10^{18} cm^{-3} in SnSe to 1.36 × 10^{19} cm^{-3} in SnSe−15%PbTe with a moderate improvement of the carrier mobility, which derives from the narrowed-bandgap and the optimization of crystal symmetry after PbTe alloying [43,45]. The decreased carrier mobility in SnSe−5%PbTe could be caused by the extra electron scattering due to additional point defects. However, as the fraction of PbTe rises, the effect of crystal symmetry promotion by PbTe alloying gradually outweighs its negative effect of point defect on carrier mobility, as shown in Fig. 2c.

Both the carrier concentration and carrier mobility increase after introducing extra Sn. The room temperature carrier concentration increases from 9.91 × 10^{18} cm^{-3} in SnSe−13%PbTe to 1.38 × 10^{19} cm^{-3} in $Sn_{1.08}$Se−13%PbTe. The room temperature carrier mobility is enhanced to 4.16 $cm^2V^{-1}s^{-1}$ in $Sn_{1.08}$Se−13% PbTe. To reconfirm the carrier mobility promotion, we carried out the weighted mobility evaluation as a function of temperature, as shown in Fig. 2d. The largely enhanced weighted mobility indicates the synergistic optimization of carrier mobility and effective mass inconsistent with the measured high hall carrier mobility and large effective mass, which will be discussed below [46].

The enhanced carrier concentration is mainly realized by

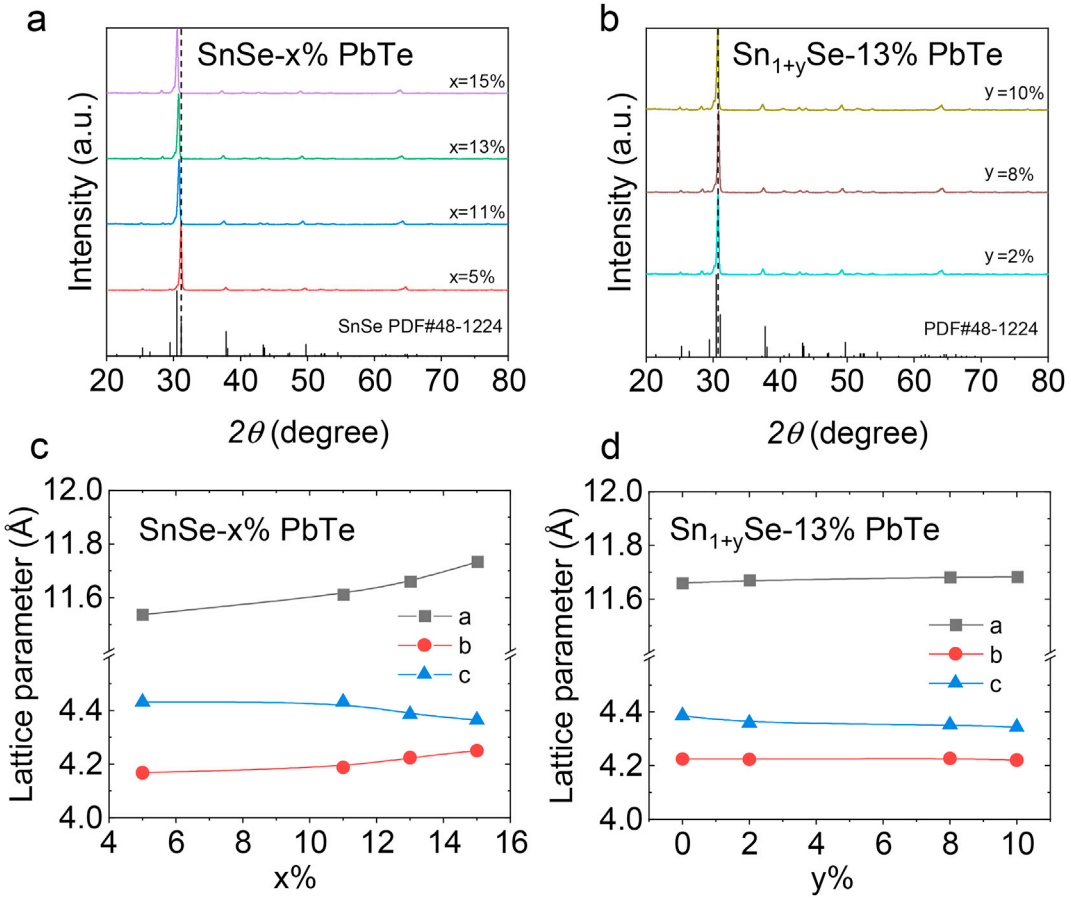

Fig. 1. Powder XRD patterns for (a) SnSe-x%PbTe (x = 0.05–0.15) and (b) $Sn_{1+y}Se$-13%PbTe (y = 0.02–0.1); and the calculated lattice parameter of (c) SnSe-x%PbTe and (d) $Sn_{1+y}Se$-13%PbTe.

reducing the impurity transition energy. Generally, the impurity transition energy in narrow-bandgap semiconductors is low because the upper limit of dopants' transition energy is the bandgap value, for example, the bandgap of PbTe is only 0.3 eV. However, the bandgap of SnSe is 0.86 eV. The wide bandgap makes impurities with high transition energy possible. In bare SnSe, the transition energy of Se vacancy is 0.76 eV [39], much higher than $3k_BT$ (0.075 eV at room temperature), indicating that Se vacancy is not an effective electron donor in SnSe. To investigate the transition energy of Br doped SnSe, we carried out DFT calculations. Table S1 shows the transition energy of *n*-type doping. It is found that Sn_i, Sn_{Se}, Br_{Se} has the transition energy of 0.354 eV, 0.216 eV and 0.131 eV, respectively. Br dopant possesses the lowest transition energy, however, its transition energy is still larger than that of Na, which is only 0.054 eV. Previous work reveals that the impurity transition level shifts in accordance with the bandgap in alloys [47,48]. Namely, the impurity transition energy increases/decreases with enlarged/narrowed bandgap, providing a powerful tool to tune the impurity transition energy. Here, we expected the bandgap will be reduced through the solid solution of SnSe–PbTe. Indeed, The UV–Vis spectroscopy reveals that the bandgap of Br-doped SnSe decreases as the fraction of PbTe from 0.84 eV to 0.74 eV in SnSe–15%PbTe, as shown in Fig. 3a. The reduced bandgap could shallow the impurity transition energy level, facilitating the activation of electrons into the conduction bands, as shown in Fig. 3b [44]. Meanwhile, as shown in our previous work, carrier mobility is related to crystal symmetry [44]. Increased crystal symmetry weakens the electron-phonon coupling and compensates for the detrimental effect of the solid solution scattering on carrier mobility. Here it is the high symmetric cubic structure of PbTe that contributes to the moderately increased carrier mobility.

To investigate the effect of extra Sn in *n*-type SnSe, the formation energy of different defects in SnSe is calculated, as shown in Fig. 4a–b. Due to the intrinsic Sn vacancies, pristine SnSe possesses a *p*-type transport feature. While the SnSe becomes an *n*-type semiconductor due to the donor impurity, Sn vacancies in *n*-type SnSe act as electron traps which reduce the electron concentration. After introducing extra Sn, the formation energy of Sn vacancy increases which indicates that the Sn vacancy amount is reduced in Sn-rich SnSe. As the fraction of extra Sn increases, extra Sn can even form Sn nanophases, as shown in Fig. 4c. Because the work function of Sn is ~4.4 eV and the electron affinity of SnSe is ~4.7eV [49], metallic Sn nanophases are able to inject electrons into the conduction band of SnSe and increase the carrier concentration. Furthermore, the Sn nanophase located near the crystal boundary, which is directly observed by SEM, could reduce the intergrain energy barrier to further enhance carrier mobility [42]. As a result, the carrier mobility and carrier concentration obtain a remarkable improvement with extra Sn.

To demonstrate the presence of extra Sn in *n*-type SnSe and its distribution, the SEM image and SEM-EDS elemental mapping of $Sn_{1.08}Se$–13%PbTe are shown in Fig. 5. The gray dotted line marks the grain boundary of *n*-type SnSe polycrystals and several second nanophases are mainly dispersed around the grain boundary, as shown in Fig. 5a. Combined with the SEM-EDS elemental mapping

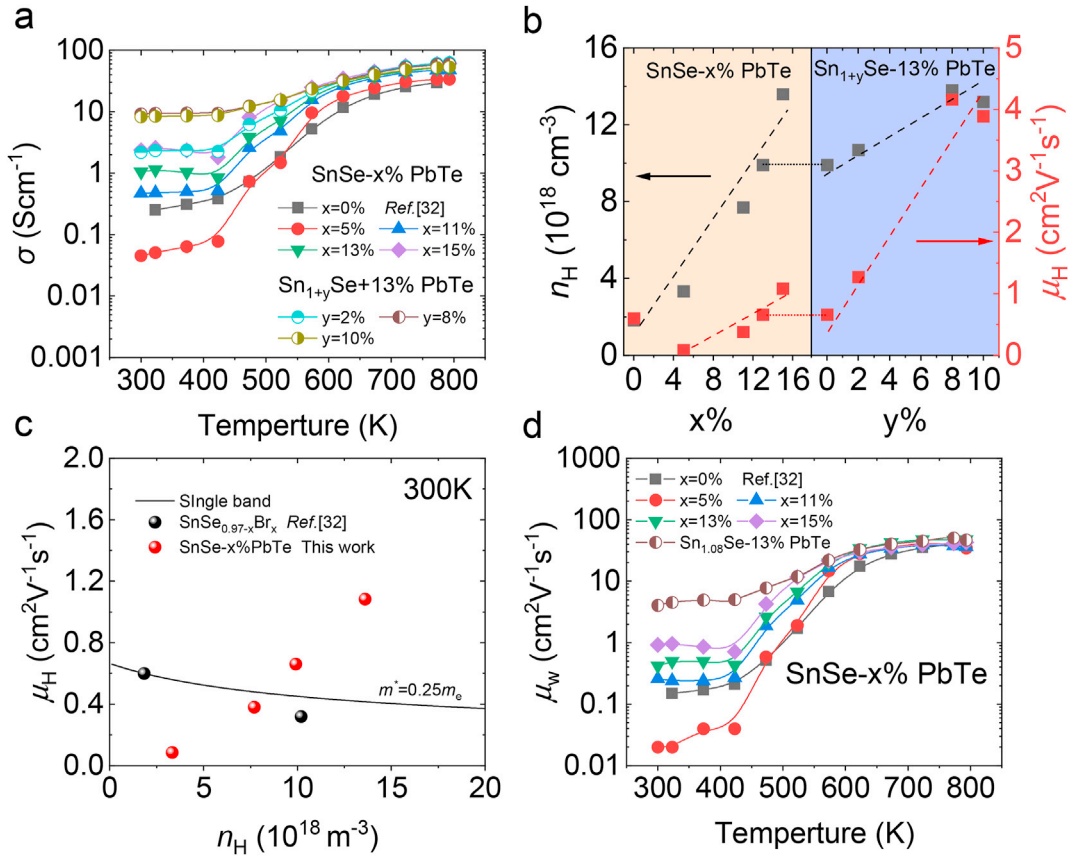

Fig. 2. The electrical transport properties of SnSe-x%PbTe and $Sn_{1+y}Se$-13%PbTe: (a) temperature-dependent electrical conductivity; (b) the room-temperature carrier mobility and carrier concentration as a function of PbTe and Sn amount; (c) the room-temperature carrier mobility as a function of the carrier concentration; (d) the temperature-dependent weighted mobility [32].

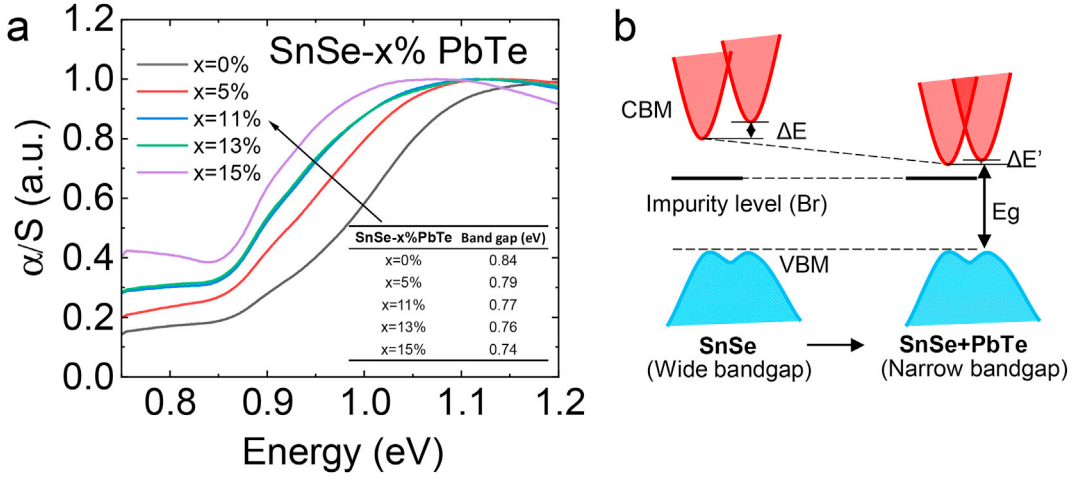

Fig. 3. (a) The bandgap of SnSe-x%PbTe; (b) schematic diagram of the band structure evolution with PbTe alloying.

of respective elements, Fig. 5b–f, it is evident that extra Sn in *n*-type SnSe forms as Sn second phase near the grain boundary.

The Seebeck coefficients of PbTe-alloyed SnSe and Sn-compensated SnSe are shown in Fig. 6a–b. Generally, the Seebeck coefficient could decrease with increasing carrier concentration according to the single parabolic band model (SPB), while no significant Seebeck reduction is observed with increasing PbTe/Sn amount. To get an insight into the abnormal Seebeck coefficient behavior, the room-temperature Pisarenko relationship has been illustrated in Fig. 6c. It is evident that the calculated SPB model with $0.56m_e$ lies below the measured Seebeck coefficients of SnSe-x% PbTe, indicating that a more complex band structure may participate in the electron transport. According to our previous work [44], we attribute it to the Pb-induced conduction band convergence, as shown in Fig. 3b. Therefore, benefitting from enhanced electrical conductivity and relatively high Seebeck coefficient, the power

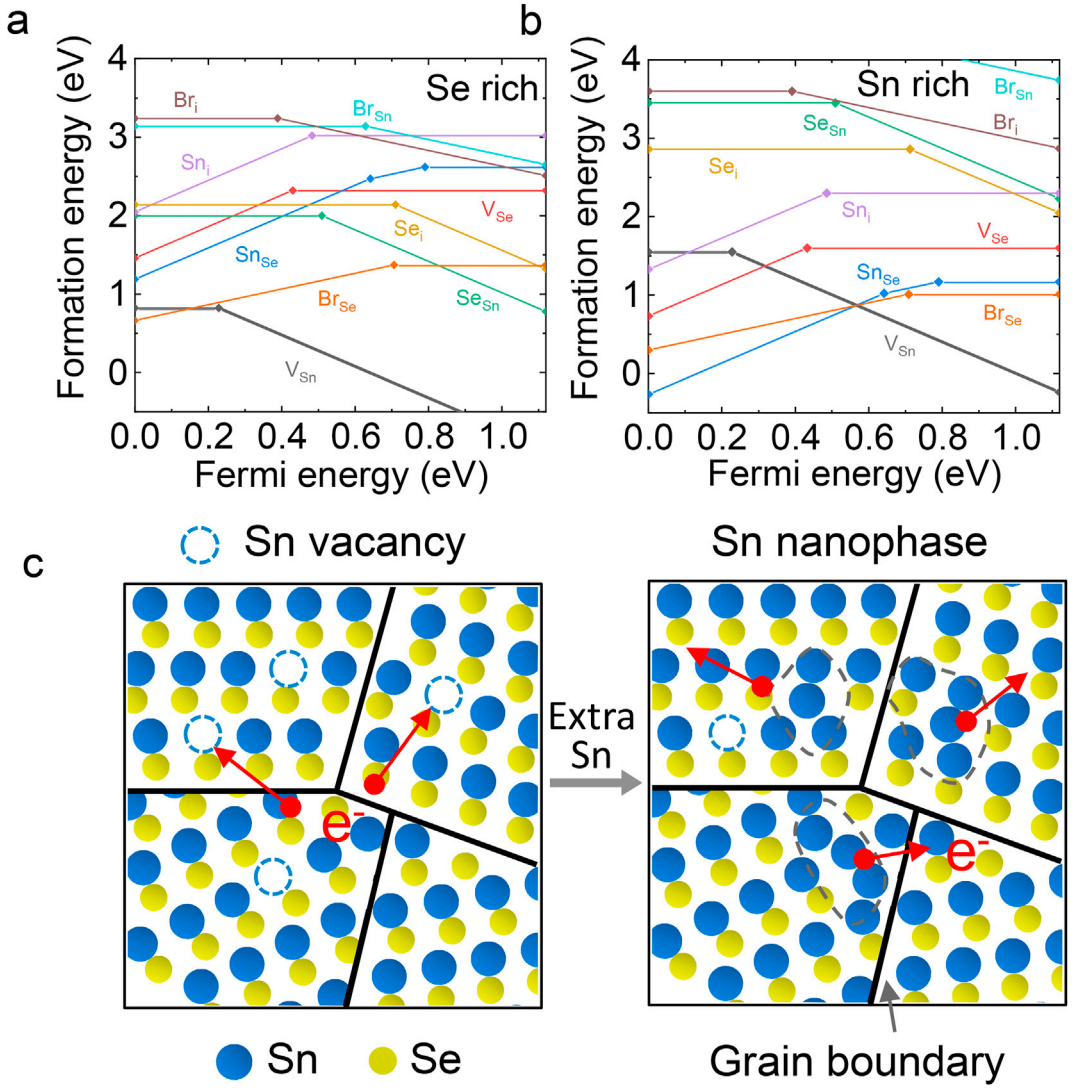

Fig. 4. The formation energy of different defects in SnSe as a function of Fermi energy in different conditions: (a) Se rich and (b) Sn rich; (c) the schematic diagram of the vacancy compensation effect with extra Sn. Data in (a) and (b) are adopted from Ref. [44].

factor in a broad temperature range is significantly enhanced, and a remarkable peak power factor of ~8.3 μWcm^{-1}K^{-2} is achieved at 793 K in $SnSe_{1.08}$-13%PbTe, which is superior to other *n*-type SnSe polycrystals [31,35,36,50].

Fig. 7a–c shows the lattice thermal conductivity (κ_{lat}) of SnSe-x %PbTe and Sn-compensated Sn_{1+y}Se-13%PbTe (The total thermal conductivity, Lorenz number, specific heat, electronic thermal conductivity and sample density can be found in Figure S3-S5 and Table S2). For SnSe-x%PbTe, the room-temperature κ_{lat}decreases with the increasing fraction of PbTe when the fraction is lower than 11% from ~0.6 Wm^{-1}K^{-1} in SnSe to 0.4 Wm^{-1}K^{-1} in SnSe–11%PbTe. This decreasing trend of κ_{lat} originated from strain and mass field fluctuations by PbTe alloying [43,44]. However, κ_{lat} begins to increase when PbTe excesses the solubility in SnSe and is even higher than SnSe in the high-temperature region. The upturned thermal conductivity in the high-temperature region is not caused by the bipolar effect. Even though the bandgap is narrowed by PbTe alloying, the narrowed bandgap such as ~0.74 eV is still wide. Furthermore, the temperature-dependent Seebeck coefficient for SnSe-x%PbTe and Sn_{1+y}Se-13%PbTe are similar to the Br-doped SnSe, as shown in Fig. 6a–b, indicating no thermal activation of the minority carriers happens. Instead, the upturned high-temperature lattice thermal conductivities could be caused by the combined effect of PbTe second phase (when PbTe excesses the solubility in SnSe) and the phase transition of SnSe from the space group *Pnma* to *Cmcm*. Although the thermal conductivity of SnSe-x %PbTe appears mild increases in the high-temperature region compared with SnSe, a relatively high *ZT* value of ~1.4 at 793 K and ZT_{ave} of ~0.46 in 300–793 K is achieved in SnSe–13%PbTe due to its enhanced power factor. For Sn-compensated SnSe, κ_{lat} in the middle and high-temperature region largely decreases with extra Sn, from 0.39 Wm^{-1}K^{-1} in SnSe–13%PbTe to 0.31 Wm^{-1}K^{-1} in $Sn_{1.1}$Se–13%PbTe at 793 K. This decrease results from the formation of Sn nanophases which may have a strong phonon scattering effect to reduce the κ_{lat}, especially in the middle and high-temperature region. Finally, the combination of improved *PF* and considerably

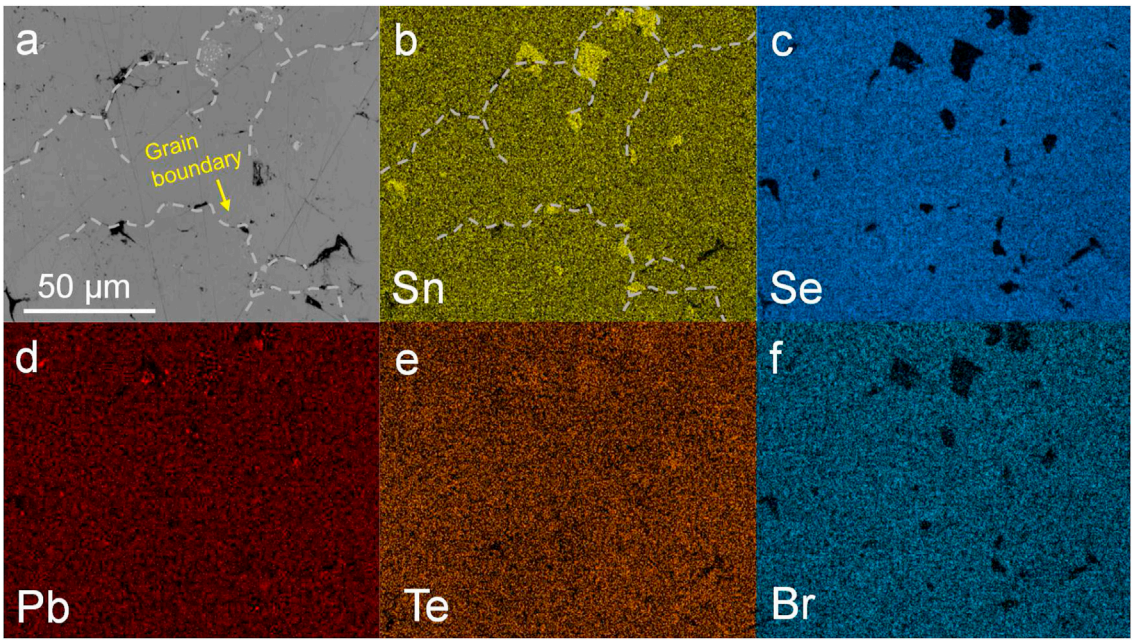

Fig. 5. (a) SEM images and (b–f) the corresponding EDS mappings of Sn, Se, Pb, Te, and Br for $Sn_{1.08}Se$-13% PbTe.

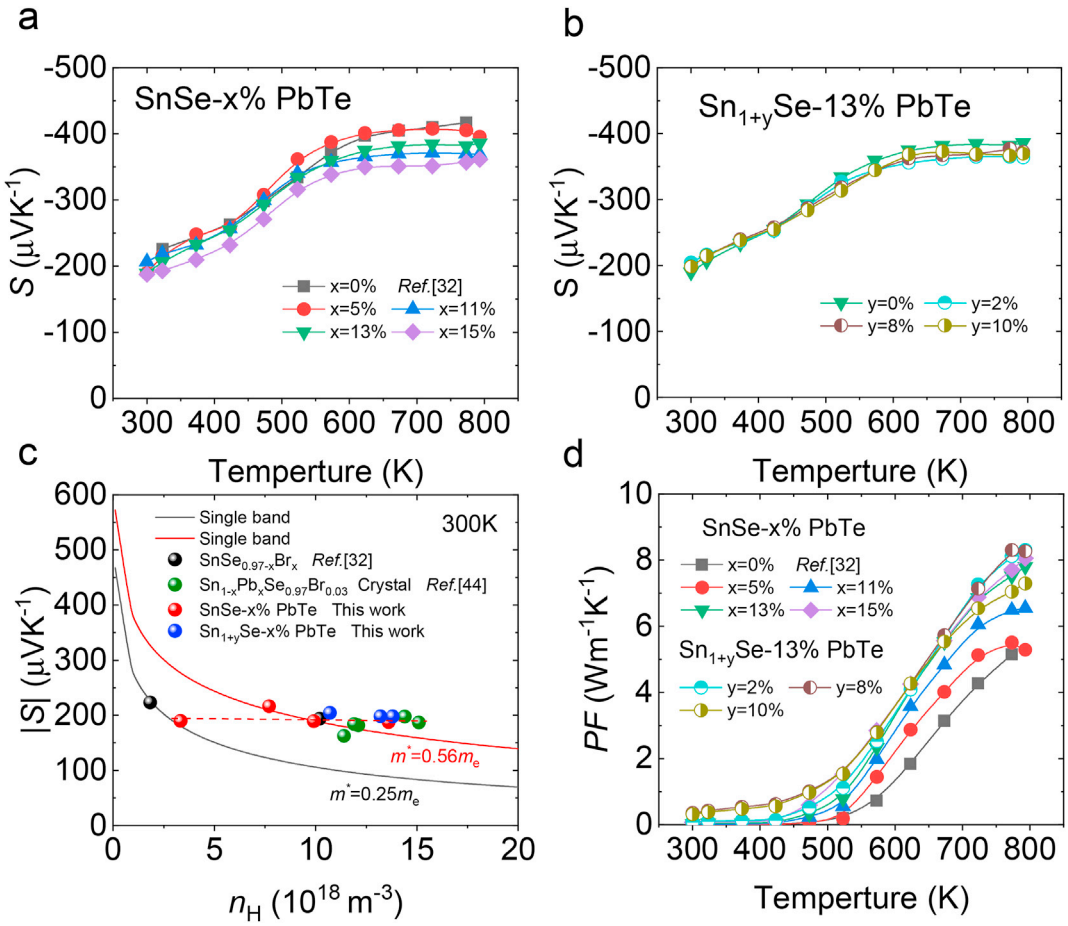

Fig. 6. Temperature-dependent Seebeck coefficient of (a) SnSe-x%PbTe and (b) $Sn_{1+y}Se$-13%PbTe; (c) Pisarenko plot and experimental date of PbTe-alloyed SnSe and other *n*-type SnSe crystal and polycrystals [44]; (d) power factor [32].

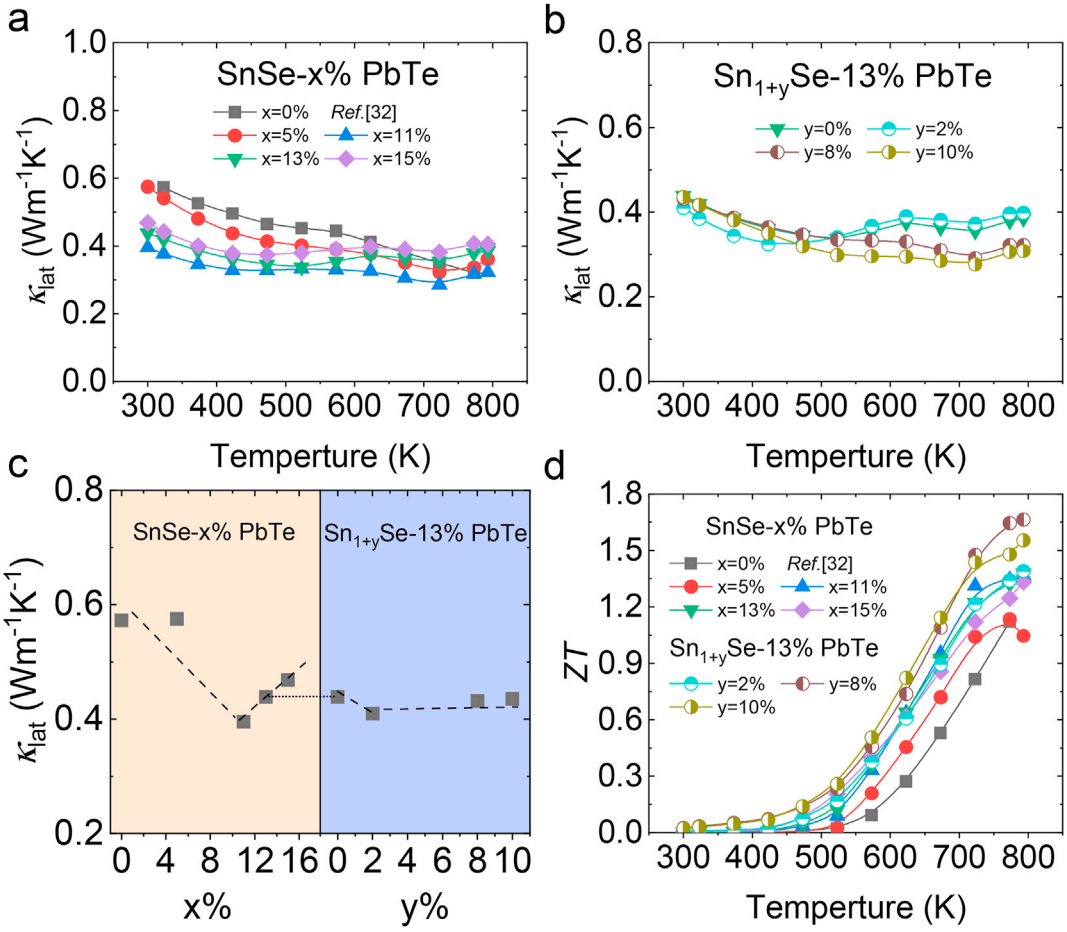

Fig. 7. Temperature-dependent κ_{lat} of (a) SnSe-x%PbTe; (b) $Sn_{1+y}Se$-13%PbTe; (c) the room-temperature κ_{lat} as a function of PbTe and Sn fractions; (d) *ZT* values [32].

reduced κ_{lat} results in a high ZT_{max} of ~1.7 at 793 K and a ZT_{ave} of ~0.58 in 300–793 K in $Sn_{1.08}Se$–13%PbTe, as shown in Fig. 7d.

3. Conclusions

In this work, the TE performance of *n*-type SnSe polycrystals is successfully optimized *via* bandgap engineering and vacancy compensation. Utilizing PbTe alloying, the bandgap of Br-doped SnSe is reduced, which shallows the impurity energy level and increases the carrier concentration from 1.8×10^{18} cm^{-3} to 1.36×10^{19} cm^{-3}. Meanwhile, the carrier mobility mildly increases due to the optimization of crystal symmetry. And the band convergence between two conduction bands with PbTe alloying also enhances the Seebeck coefficient. As a result, a maximum $ZT \approx 1.4$ at 793 K is obtained in SnSe–13%PbTe. Furthermore, we introduced extra Sn to promote the TE performance of SnSe-13% PbTe. Firstly, extra Sn can compensate the intrinsic Sn vacancies and form the Sn nanophase which could donate electrons to enhance the carrier concentration. Secondly, Sn nanophases could introduce strong phonon scattering to reduce κ_{lat}. Also, Sn nanophases located near the crystal boundary could reduce the intergrain energy barrier to improve the carrier mobility. Finally, a remarkable ZT_{max} of ~1.7 at 793 K and ZT_{ave} of 0.58 in 300–793 K are obtained in $Sn_{1.08}Se$–13%PbTe. Our findings provide a deep insight into the electrical and thermal transport behaviors in SnSe, and pave a way to promote the TE performance of other wide-bandgap semiconductors.

4. Experimental section

High-pure raw materials (Sn, Se, Pb, Te, and $SnBr_2$) were weighted in a stoichiometric ratio of $Sn_{1-x}Pb_xSe_{0.97-x}Te_xBr_{0.03}$ (x = 5%, 11%, 13%, 15%) and $Sn_{0.87+y}Pb_{0.13}Se_{0.84}Te_{0.13}Br_{0.03}$ (y = 2%, 8%, 10%) and then loaded into silica tubes. The tubes were flame-sealed under a pressure of 10^{-4} torr and then put into the furnace and heated to obtain the ingots. The ingots were put into an N_2-filled glove box and ground into powder. The powder was sintered by SPS to obtain densified samples. The powder X-ray diffraction (PXRD) patterns were obtained with Cu Kα (λ = 1.5418 Å). Scanning electron microscopy (SEM) and energy dispersive X-ray spectroscopy (EDS) studies were conducted using a Schottky Field Emission Scanning Electron Microscope (SFESEM, JEOL, JSM 7900F) in the Center for High Pressure Science and Technology Advanced Research (HPSTAR). The Hall coefficients (R_H) were measured with a Lake Shore 8400 Series system and the carrier concentration was calculated by $n_H = 1/(eR_H)$. The optical bandgap was measured with a UV–vis–NIR Spectrophotometer (UV-3600 Plus) equipped with a polytetrafluoroethylene (PTFE) integrating sphere. The electrical conductivity and the Seebeck coefficient were measured with an Ulvac Riko ZEM-3 instrument. The thermal diffusivity was measured with a Netzsch LFA457 instrument. More experimental details and other measured data and are provided in Supporting Information (SI).

Credit author statement

Lizhong Su: synthesized the samples, designed and carried out the experiments, analyzed the results and wrote the paper, conceived the experiments, analyzed the results and co-edited the manuscript. Tao Hong: carried out the TEM experiments, conceived the experiments, analyzed the results and co-edited the manuscript. Dongyang Wang: carried out the DFT calculations, conceived the experiments, analyzed the results and co-edited the manuscript. Sining Wang: carried out the Hall measurements, conceived the experiments, analyzed the results and co-edited the manuscript. Bingchao Qin: carried out the Hall measurements, conceived the experiments, analyzed the results and co-edited the manuscript. Mengmeng Zhang: synthesized the samples, designed and carried out the experiments, analyzed the results and wrote the paper, conceived the experiments, analyzed the results and co-edited the manuscript. Xiang Gao: carried out the TEM experiments, conceived the experiments, analyzed the results and co-edited the manuscript. Cheng Chang: synthesized the samples, designed and carried out the experiments, analyzed the results and wrote the paper, conceived the experiments, analyzed the results and co-edited the manuscript. Li-Dong Zhao: synthesized the samples, designed and carried out the experiments, analyzed the results and wrote the paper, conceived the experiments, analyzed the results and co-edited the manuscript.

Declaration of competing interest

Authors declare no any interests in this work.

Acknowledgments

This work was supported by National Natural Science Foundation of China (51772012), National Key Research and Development Program of China (2018YFA0702100 and 2018YFB0703600), the Beijing Natural Science Foundation (JQ18004). This work was also supported by Lise Meitner Project (M2889-N) and the National Postdoctoral Program for Innovative Talents (BX20200028). L.D.Z. appreciates the support of the High Performance Computing (HPC) resources at Beihang University, the National Science Fund for Distinguished Young Scholars (51925101), and center for High Pressure Science and Technology Advanced Research (HPSTAR) for SEM measurements.

Appendix A. Supplementary data

Supplementary data to this article can be found online at https://doi.org/10.1016/j.mtphys.2021.100452.

References

[1] G. Tan, L.D. Zhao, M.G. Kanatzidis, Rationally designing high-performance bulk thermoelectric materials, Chem. Rev. 116 (2016) 12123–12149, https://doi.org/10.1021/acs.chemrev.6b00255.
[2] X.L. Shi, J. Zou, Z.G. Chen, Advanced thermoelectric design: from materials and structures to devices, Chem. Rev. 120 (15) (2020) 7399–7515, https://doi.org/10.1021/acs.chemrev.0c00026.
[3] W. Liu, J. Hu, S. Zhang, M. Deng, C.-G. Han, Y. Liu, New trends, strategies and opportunities in thermoelectric materials: a perspective, Mater. Today Phys. 1 (2017) 50–60, https://doi.org/10.1016/j.mtphys.2017.06.001.
[4] Y. Zhou, H. Wu, D. Wang, L. Fu, Y. Zhang, J. He, S.J. Pennycook, L.D. Zhao, Investigations on electrical and thermal transport properties of Cu_2SnSe_3 with unusual coexisting nanophases, Mater. Today Phys. 7 (2018) 77–88, https://doi.org/10.1016/j.mtphys.2018.11.001.
[5] X. Zhang, L.D. Zhao, Thermoelectric materials: energy conversion between heat and electricity, J. Materiomics 1 (2) (2015) 92–105, https://doi.org/10.1016/j.jmat.2015.01.001.
[6] W. Liu, X. Tan, K. Yin, H. Liu, X. Tang, J. Shi, Q. Zhang, C. Uher, Convergence of conduction bands as a means of enhancing thermoelectric performance of n-type $Mg_2Si_{1-x}Sn_x$ solid solutions, Phys. Rev. Lett. 108 (16) (2012) 166601, https://doi.org/10.1103/PhysRevLett.108.166601.
[7] Y. Xiao, D. Wang, Y. Zhang, C. Chen, S. Zhang, K. Wang, G. Wang, S.J. Pennycook, G.J. Snyder, H. Wu, L.D. Zhao, Band sharpening and band Alignment enable high quality factor to enhance thermoelectric performance in n-type PbS, J. Am. Chem. Soc. 142 (8) (2020) 4051–4060, https://doi.org/10.1021/jacs.0c00306.
[8] J.P. Heremans, V. Jovovic, E.S. Toberer, A. Saramat, K. Kurosaki, A. Charoenphakdee, S. Yamanaka, G.J. Snyder, Enhancement of thermoelectric efficiency in PbTe by distortion of the electronic density of states, Science 321 (5888) (2008) 554–557, https://doi.org/10.1126/science.1159725.
[9] L.D. Zhao, J. He, S. Hao, C.I. Wu, T.P. Hogan, C. Wolverton, V.P. Dravid, M.G. Kanatzidis, Raising the thermoelectric performance of p-type PbS with endotaxial nanostructuring and valence-band offset engineering using CdS and ZnS, J. Am. Chem. Soc. 134 (39) (2012) 16327–16336, https://doi.org/10.1021/ja306527n.
[10] K. Biswas, J. He, I.D. Blum, C.-I. Wu, T.P. Hogan, D.N. Seidman, V.P. Dravid, M.G. Kanatzidis, High-performance bulk thermoelectrics with all-scale hierarchical architectures, Nature 489 (7416) (2012) 414–418, https://doi.org/10.1038/nature11439.
[11] Y.L. Pei, G.J. Tan, D. Feng, L. Zheng, Q. Tan, X.B. Xie, S.K. Gong, Y. Chen, J.F. Li, J.Q. He, M.G. Kanatzidis, L.D. Zhao, Integrating band structure engineering with all-scale hierarchical structuring for high thermoelectric performance in PbTe system, Adv. Energy Mater. 7 (3) (2017) 1601450, https://doi.org/10.1002/aenm.201601450.
[12] H. Kang, Z. Yang, X. Yang, J. Li, W. He, Z. Chen, E. Guo, L.D. Zhao, T. Wang, Preparing bulk Cu-Ni-Mn based thermoelectric alloys and synergistically improving their thermoelectric and mechanical properties using nanotwins and nanoprecipitates, Mater. Today Phys. 17 (2021) 100332, https://doi.org/10.1016/j.mtphys.2020.100332.
[13] X. Materials Today PhysicsQian, H. Wu, D. Wang, Y. Zhang, S.J. Pennycook, X. Gao, L. Zheng, L.D. Zhao, Synergistically optimizing interdependent thermoelectric parameters of n-type PbSe through introducing a small amount of Zn, Mater. Today Phys. 9 (2019) 100102, https://doi.org/10.1016/j.mtphys.2019.100102.
[14] S.N. Wang, Y. Xiao, D.D. Ren, L.Z. Su, Y.T. Qiu, L.D. Zhao, Enhancing thermoelectric performance of $BiSbSe_3$ through improving carrier mobility via percolating carrier transports, J. Alloys Compd. 836 (2020) 155473, https://doi.org/10.1016/j.jallcom.2020.155473.
[15] L.D. Zhao, S.H. Lo, Y. Zhang, H. Sun, G. Tan, C. Uher, C. Wolverton, V.P. Dravid, M.G. Kanatzidis, Ultralow thermal conductivity and high thermoelectric figure of merit in SnSe crystals, Nature 508 (7496) (2014) 373–377, https://doi.org/10.1038/nature13184.
[16] W. He, D. Wang, H. Wu, Y. Xiao, Y. Zhang, D. He, Y. Feng, Y.J. Hao, J.F. Dong, R. Chetty, L. Hao, D. Chen, J. Qin, Q. Yang, X. Li, J.M. Song, Y. Zhu, W. Xu, C. Niu, X. Li, G. Wang, C. Liu, M. Ohta, S.J. Pennycook, J. He, J.F. Li, L.D. Zhao, High thermoelectric performance in low-cost $SnS_{0.91}Se_{0.09}$ crystals, Science 365 (6460) (2019) 1418–1424, https://doi.org/10.1126/science.aax5123.
[17] X. Zhang, C. Chang, Y. Zhou, L.D. Zhao, BiCuSeO thermoelectrics: an update on recent progress and perspective, Materials 10 (2) (2017) 198, https://doi.org/10.3390/ma10020198.
[18] K. Biswas, L.D. Zhao, M.G. Kanatzidis, Tellurium-free thermoelectric: the anisotropic n-type semiconductor Bi_2S_3, Adv. Energy Mater. 2 (6) (2012) 634–638, https://doi.org/10.1002/aenm.201100775.
[19] M.K. Jana, K. Pal, U.V. Waghmare, K. Biswas, The origin of ultralow thermal conductivity in InTe: lone-pair-induced anharmonic rattling, Angew Chem. Int. Ed. Engl. 55 (27) (2016) 7792–7796, https://doi.org/10.1002/anie.201511737.
[20] C. Chang, L.D. Zhao, Anharmoncity and low thermal conductivity in thermoelectrics, Mater. Today Phys. 4 (2018) 50–57, https://doi.org/10.1016/j.mtphys.2018.02.005.
[21] J. He, T.M. Tritt, Advances in thermoelectric materials research: looking back and moving forward, Science 357 (6358) (2017): eaak9997, https://doi.org/10.1126/science.aak9997.
[22] Y. Xiao, L.D. Zhao, Seeking new, highly effective thermoelectrics, Science 367 (6483) (2020) 1196–1197, https://doi.org/10.1126/science.aaz9426.
[23] H. Wang, Y. Pei, A.D. Lalonde, G.J. Snyder, Weak electron-phonon coupling contributing to high thermoelectric performance in n-type PbSe, Proc. Natl. Acad. Sci. U.S.A. 109 (25) (2012) 9705–9709, https://doi.org/10.1073/pnas.1111419109.
[24] S. Li, Y. Wang, C. Chen, X. Li, W. Xue, X. Wang, Z. Zhang, F. Cao, J. Sui, X. Liu, Q. Zhang, Heavy doping by bromine to improve the thermoelectric properties of n-type polycrystalline SnSe, Adv. Sci. 5 (9) (2018) 1800598, https://doi.org/10.1002/advs.201800598.
[25] Y. Xiao, C. Chang, Y.L. Pei, D. Wu, K.L. Peng, X.Y. Zhou, S.K. Gong, J.Q. He, Y.S. Zhang, Z. Zeng, L.D. Zhao, Origin of low thermal conductivity in SnSe, Phys. Rev. B 94 (12) (2016) 125203, https://doi.org/10.1103/PhysRevB.94.125203.
[26] L.D. Zhao, V.P. Dravid, M.G. Kanatzidis, The panoscopic approach to high performance thermoelectrics, Energy Environ. Sci. 7 (1) (2014) 251–268, https://doi.org/10.1039/c3ee43099e.
[27] L.D. Zhao, G. Tan, S. Hao, J. He, Y. Pei, H. Chi, H. Wang, S. Gong, H. Xu, V.P. Dravid, C. Uher, G.J. Snyder, C. Wolverton, M.G. Kanatzidis, Ultrahigh power factor and thermoelectric performance in hole-doped single-crystal SnSe, Science 351 (6269) (2016) 141–144, https://doi.org/10.1126/

science.aad3749.
[28] C. Chang, M. Wu, D. He, Y. Pei, C.F. Wu, X. Wu, H. Yu, F. Zhu, K. Wang, Y. Chen, L. Huang, J.F. Li, J. He, L.D. Zhao, 3D charge and 2D phonon transports leading to high out-of-plane ZT in n-type SnSe crystals, Science 360 (6390) (2018) 778–783, https://doi.org/10.1126/science.aaq1479.
[29] B. Qin, Y. Zhang, D. Wang, Q. Zhao, B. Gu, H. Wu, H. Zhang, B. Ye, S.J. Pennycook, L.D. Zhao, Ultrahigh average ZT realized in p-type SnSe crystalline thermoelectrics through producing extrinsic vacancies, J. Am. Chem. Soc. 142 (12) (2020) 5901–5909, https://doi.org/10.1021/jacs.0c01726.
[30] L.S. Mao, Y.N. Yin, Q. Zhang, G.Q. Liu, H.X. Wang, Z. Guo, H.Y. Hu, Y.K. Xiao, X.J. Tan, J. Jiang, Fermi-surface dynamics and high thermoelectric performance along the out-of-plane direction in n-type SnSe crystals, Energy Environ. Sci. 13 (2) (2020) 616–621, https://doi.org/10.1039/c9ee03897c.
[31] Q. Zhang, E.K. Chere, J. Sun, F. Cao, K. Dahal, S. Chen, G. Chen, Z. Ren, Studies on thermoelectric properties of n-type polycrystalline $SnSe_{1-x}S_x$ by iodine doping, Adv. Energy Mater. 5 (12) (2015) 1500360, https://doi.org/10.1002/aenm.201500360.
[32] C. Chang, Q. Tan, Y.L. Pei, Y. Xiao, X. Zhang, Y.X. Chen, L. Zheng, S.K. Gong, J.F. Li, J.Q. He, L.D. Zhao, Raising thermoelectric performance of n-type SnSe via Br doping and Pb alloying, RSC Adv. 6 (100) (2016) 98216–98220, https://doi.org/10.1039/c6ra21884a.
[33] Y.K. Lee, K. Ahn, J. Cha, C. Zhou, H.S. Kim, G. Choi, S.I. Chae, J.H. Park, S.P. Cho, S.H. Park, Y.E. Sung, W.B. Lee, T. Hyeon, I. Chung, Enhancing p-type thermoelectric performances of polycrystalline SnSe via tuning phase transition temperature, J. Am. Chem. Soc. 139 (31) (2017) 10887–10896, https://doi.org/10.1021/jacs.7b05881.
[34] X. Shi, K. Zheng, M. Hong, W. Liu, R. Moshwan, Y. Wang, X. Qu, Z.-G. Chen, J. Zou, Boosting the thermoelectric performance of p-type heavily Cu-doped polycrystalline SnSe via inducing intensive crystal imperfections and defect phonon scattering, Chem. Sci. 9 (37) (2018) 7376–7389, https://doi.org/10.1039/c8sc02397b.
[35] P.P. Shang, J. Dong, J. Pei, F.H. Sun, Y. Pan, H. Tang, B.P. Zhang, L.D. Zhao, J.F. Li, Highly textured N-type SnSe polycrystals with enhanced thermoelectric performance, Research (2019) 9253132, https://doi.org/10.34133/2019/9253132.
[36] Z.H. Ge, Y. Qiu, Y.X. Chen, X. Chong, J. Feng, Z.K. Liu, J. He, Multipoint defect synergy realizing the excellent thermoelectric performance of n-type polycrystalline SnSe via Re doping, Adv. Funct. Mater. 29 (28) (2019) 1902893, https://doi.org/10.1002/adfm.201902893.
[37] C. Li, H. Wu, B. Zhang, H. Zhu, Y. Fan, X. Lu, X. Sun, X. Zhang, G. Wang, X. Zhou, High thermoelectric performance of Co-doped P-type polycrystalline SnSe via optimizing electrical transport properties, ACS Appl. Mater. Interfaces 12 (7) (2020) 8446–8455, https://doi.org/10.1021/acsami.9b20610.
[38] W. Wei, C. Chang, T. Yang, J. Liu, H. Tang, J. Zhang, Y. Li, F. Xu, Z. Zhang, J.F. Li, G. Tang, Achieving high thermoelectric figure of merit in polycrystalline SnSe via introducing Sn vacancies, J. Am. Chem. Soc. 140 (1) (2018) 499–505, https://doi.org/10.1021/jacs.7b11875.
[39] Y. Zhou, W. Li, M. Wu, L.D. Zhao, J. He, S.H. Wei, L. Huang, Influence of defects on the thermoelectricity in SnSe: a comprehensive theoretical study, Phys. Rev. B 97 (2018) 245202, https://doi.org/10.1103/PhysRevB.97.245202.
[40] J. Ma, S.H. Wei, T.A. Gessert, K.K. Chin, Carrier density and compensation in semiconductors with multiple dopants and multiple transition energy levels: case of Cu impurities in CdTe, Phys. Rev. B 83 (24) (2011) 245207, https://doi.org/10.1103/PhysRevB.83.245207.
[41] T.R. Wei, G. Tan, X. Zhang, C.F. Wu, J.F. Li, V.P. Dravid, G.J. Snyder, M.G. Kanatzidis, Distinct impact of alkali-ion doping on electrical transport properties of thermoelectric p-type polycrystalline SnSe, J. Am. Chem. Soc. 138 (2016) 8875–8882, https://doi.org/10.1021/jacs.6b04181.
[42] M. Ibáñez, Z. Luo, A. Genç, L. Piveteau, S. Ortega, D. Cadavid, O. Dobrozhan, Y. Liu, M. Nachtegaal, M. Zebarjadi, J. Arbiol, M.V. Kovalenko, A. Cabot, High-performance thermoelectric nanocomposites from nanocrystal building blocks, Nat. Commun. 7 (1) (2016) 10766, https://doi.org/10.1038/ncomms10766.
[43] B. Qin, D. Wang, W. He, Y. Zhang, H. Wu, S.J. Pennycook, L.D. Zhao, Realizing high thermoelectric performance in p-type SnSe through crystal structure modification, J. Am. Chem. Soc. 141 (2) (2019) 1141–1149, https://doi.org/10.1021/jacs.8b12450.
[44] C. Chang, D. Wang, D. He, W. He, F. Zhu, G. Wang, J. He, L.D. Zhao, Realizing high-ranged out-of-plane ZTs in N-type SnSe crystals through promoting continuous phase transition, Adv. Energy Mater. 9 (28) (2019) 1901334, https://doi.org/10.1002/aenm.201901334.
[45] J. Wang, R. Zhao, M. Yang, Z. Liu, Z. Liu, Inverse relationship between carrier mobility and bandgap in graphene, J. Chem. Phys. 138 (8) (2013): 084701, https://doi.org/10.1063/1.4792142.
[46] G.J. Snyder, A.H. Snyder, M. Wood, R. Gurunathan, B.H. Snyder, C. Niu, Weighted mobility, Adv. Mater. 32 (25) (2020): e2001537, https://doi.org/10.1002/adma.202001537.
[47] E.P. Skipetrov, E.A. Zvereva, V.V. Belousov, L.A. Skipetrova, E.I. Slyn'ko, Gallium-induced deep level in $Pb_{1-x}Ge_xTe$ alloys, Semiconductors 34 (8) (2000) 894–896, https://doi.org/10.1134/1.1188096.
[48] V. Jovovic, S.J. Thiagarajan, J.P. Heremans, T. Komissarova, D. Khokhlov, A. Nicorici, Low temperature thermal, thermoelectric, and thermomagnetic transport in indium rich $Pb_{1-x}Sn_xTe$ alloys, J. Appl. Phys. 103 (5) (2008): 053710, https://doi.org/10.1063/1.2890150.
[49] V.R. Minnam Reddy, S. Gedi, B. Pejjai, C. Park, Perspectives on SnSe-based thin film solar cells: a comprehensive review, J. Mater. Sci. Mater. Electron. 27 (6) (2016) 5491–5508, https://doi.org/10.1007/s10854-016-4563-9.
[50] J. Cai, Y. Zhang, Y. Yin, X. Tan, S. Duan, G.-Q. Liu, H. Hu, Y. Xiao, Z. Ge, J. Jiang, Investigating the thermoelectric performance of n-type SnSe: the synergistic effect of $NbCl_5$ doping and dislocation engineering, J. Mater. Chem. C 8 (38) (2020) 13244–13252, https://doi.org/10.1039/d0tc02959a.